

A geometric path towards excitonic insulators with purely orbital time-reversal symmetry breaking

Giacomo Mazza^{1,2,*} and Marco Polini^{1,3,4}

¹*Dipartimento di Fisica dell'Università di Pisa, Largo Bruno Pontecorvo 3, I-56127 Pisa, Italy*

²*Department of Quantum Matter Physics, University of Geneva,
Quai Ernest-Ansermet 24, 1211 Geneva, Switzerland*

³*Istituto Italiano di Tecnologia, Graphene Labs, Via Morego 30, I-16163 Genova, Italy*

⁴*ICFO-Institut de Ciències Fotòniques, The Barcelona Institute of Science and Technology,
Av. Carl Friedrich Gauss 3, 08860 Castelldefels (Barcelona), Spain*

Crystalline exciton insulators are elusive states of matter whose ground state is a charge-density symmetry-broken (CDSB) state. In such a state of matter, the electronic charge distribution has a symmetry that is different from the one of the underlying crystal. An excitonic instability of purely electronic origin is therefore inevitably coupled to lattice degrees of freedom. However, an excitonic instability can also lead to an excited state displaying broken time-reversal symmetry and a persistent current. In this Letter we show a geometric path that lowers the barrier between the CDSB state and the time-reversal symmetry broken (TRSB) state. For systems in a cylindrical geometry, and for a critical cylinder radius, the magnetic flux sourced by the persistent current stabilizes the TRSB state. Our results pave the way for achieving exotic orbital magnetic order in quantum materials in a controlled fashion, and are relevant for the control of coupled structural and excitonic phase transitions.

Introduction.—In an excitonic phase transition, electronic states belonging to valence and conduction bands spontaneously hybridize due to the Coulomb interaction between negatively charged electrons and positively charged holes. Heterostructures with spatially separated electrons and holes, often under strong magnetic fields [1–5] (see, however, Ref. [6]), have been demonstrated so far to be the best systems for studying this phenomenon. Indeed, the observation of excitonic condensation in a crystalline solid remains a debated question [7–12]. Crystalline solids lack a continuous symmetry that independently conserves the number of particles and holes. This fact hinders excitonic condensation, and reduces the excitonic instability to a proxy for the breaking of discrete symmetries of the solid. Coupling to order parameters with the same symmetry can easily mask the origin of the instability. For example, the excitonic instability often induces a distortion of the charge density with respect to the underlying lattice [13]. As recently discussed in the case of Ta₂NiSe₅, the excitonic instability may therefore become practically indistinguishable from a structural phase transition [14–19] due to the coupling between the electronic and the ionic degrees of freedom. Disentangling the excitonic nature from the structural one remains a major challenge. Recent attempts in this direction are mainly focused on the use of time-dependent probes [20–22].

In this Letter, we propose an alternative, equilibrium, route, which is based on two, seemingly dichotomic, physical manifestations of the excitonic instability. Indeed, the charge-density symmetry-broken (CDSB) state is not the only possible outcome of an excitonic instability. Simple arguments of quantum mechanics show that hybridization between electronic states of different sym-

metry can also result in a charge symmetric but time-reversal symmetry-broken (TRSB) state [23, 24]. For example, for two electronic states $\Psi_e(\mathbf{x}) = \Psi_e(-\mathbf{x})$ and $\Psi_o(\mathbf{x}) = -\Psi_o(-\mathbf{x})$, which are even and odd, respectively, under inversion symmetry, the excitonic instability corresponds to the formation of an hybridized state $\Psi(\mathbf{x}) \sim \Psi_e(\mathbf{x}) + |\Delta|e^{i\varphi}\Psi_o(\mathbf{x})$. By computing the charge $\rho(\mathbf{x}) \equiv \Psi^*(\mathbf{x})\Psi(\mathbf{x})$ and momentum $\mathbf{p}(\mathbf{x}) \equiv -i\hbar\Psi^*(\mathbf{x})\nabla\Psi(\mathbf{x})$ densities, it is straightforward to see that the nature of the symmetry broken state described by $\Psi(\mathbf{x})$ depends on the phase φ . For $\varphi = \delta, \pi + \delta$, where δ is the relative phase between the even and odd wave-functions, $\Psi(\mathbf{x})$ corresponds to a CDSB state, $\rho(\mathbf{x}) \neq \rho(-\mathbf{x})$, which displays time-reversal symmetry, $\mathbf{p}(\mathbf{x}) = -\mathbf{p}(\mathbf{x})$. On the contrary, for $\varphi = \pm\frac{\pi}{2} + \delta$, it corresponds to a TRSB state, $\mathbf{p}(\mathbf{x}) \neq -\mathbf{p}(\mathbf{x})$, with a symmetric charge density $\rho(\mathbf{x}) = \rho(-\mathbf{x})$. For a generic $\varphi - \delta \neq 0, \pi, \pm\frac{\pi}{2}$, $\Psi(\mathbf{x})$ is at the same time a CDSB and TRSB state.

In this work we propose a geometric path that unmasks the excitonic insulating nature of a CDSB ground state by enabling the coupling between the TRSB excitonic state and magnetostatic degrees of freedom of the free-space electromagnetic field. Our recipe consists in bending the crystalline material harboring the CDSB excitonic insulating state into a cylindrical geometry. In such a geometry, we show that the ground state changes nature from a CDSB state to a TRSB one for a sufficiently large value of the cylinder radius.

For illustration purposes, we consider a model of interacting fermions on a two-dimensional (2D) square lattice, which displays an excitonic instability that breaks the reflection symmetries of the lattice. For such a purely electronic instability, the excitonic ground state corresponds to the pure CDSB state, whereas the TRSB one

is unstable. By exploiting the fact that the energy of a current-carrying state is lowered by the sourcing of a magnetic field, we show that, in a cylindrical geometry, the ground state shifts from the CDSB to TRSB due to the magnetic flux generated by the equilibrium persistent currents in the TRSB state. We predict the shift to occur for cylinders whose radius is larger than a critical value, which can be further controlled by an applied external flux.

In contrast to the standard CDSB realization of the excitonic instability, the TRSB state is charge symmetric and its energy can be controlled by an external magnetic flux. We therefore suggest that our results are relevant for the control of entangled structural and excitonic instabilities. *Model and purely electronic instability.*—We build a model of interacting electrons on a lattice by considering a 2D potential with the periodicity of a square lattice, $V(\mathbf{x}) = V(\mathbf{x} + \mathbf{R})$. The crystalline potential $V(\mathbf{x}) = \sum_{\mathbf{R},a} v_a(\mathbf{x} - \mathbf{R})$ originates from atomic-like potential wells $v_a(\mathbf{x} - \mathbf{R})$ centered at the position of an atom of type a in the unit cell \mathbf{R} . Specifically, we consider two atoms $a = A, A'$ per unit cell, arranged as in Fig. 1(a). We choose atomic potentials of the Yukawa type, i.e. $v_a(\mathbf{x}) = -\gamma_a e^{-|\mathbf{x}|/\xi_a} / (|\mathbf{x}| + \eta_a)$, where η_a is a short-distance cut-off. We adjust the parameters γ_a, ξ_a , and η_a in order to obtain a band structure with low-energy bands occurring in a window of width $W \sim 4$ eV, overlapping close to the Fermi level, and originating from atomic-like orbitals of different symmetry—see Fig. 1(b). In this work we consider spinless fermions and an excitonic instability that occurs only in the spin symmetric channel [25].

By assuming four electrons per unit cell, the lowest three energy bands originate from one s -like orbital and two $p_{\pm} = p_{x \pm iy}$ -like orbitals of the central atom. We derive localized Wannier wavefunctions using the projection method [26] and write the single-particle band Hamiltonian in the Wannier basis as $\mathcal{H}_0 = \sum_{\mathbf{R}, \mathbf{R}'} \sum_{\alpha, \beta = s, p_{\pm}} h_{\mathbf{R}, \mathbf{R}'}^{\alpha\beta} c_{\mathbf{R}, \alpha}^{\dagger} c_{\mathbf{R}', \beta}$. The Wannier wavefunctions are mainly localized on the central atom, with weaker amplitude on the corner atoms—see Fig. 1(c). The s -like wave-function is even under reflection with respect to the two axes $y = \pm x$, whereas the p_{\pm} -like ones are odd/even under reflections with respect to the $y = \pm x / \mp x$ axes, respectively.

Due to the above symmetries, the local matrix elements of the single-particle Hamiltonian \mathcal{H}_0 between s - and p -like orbitals identically vanish, i.e. $h_{\mathbf{R}, \mathbf{R}}^{sp_{\pm}} = 0$, implying a vanishing local hybridization between s and p_{\pm} Wannier wave-functions:

$$\Delta_{\pm}^{(0)} \equiv \langle c_{\mathbf{R}, s}^{\dagger} c_{\mathbf{R}, p_{\pm}} \rangle = 0. \quad (1)$$

The hybridizations in Eq. (1) play the role of order parameters for the breaking of the symmetries of the square lattice due to the excitonic instability. With this target

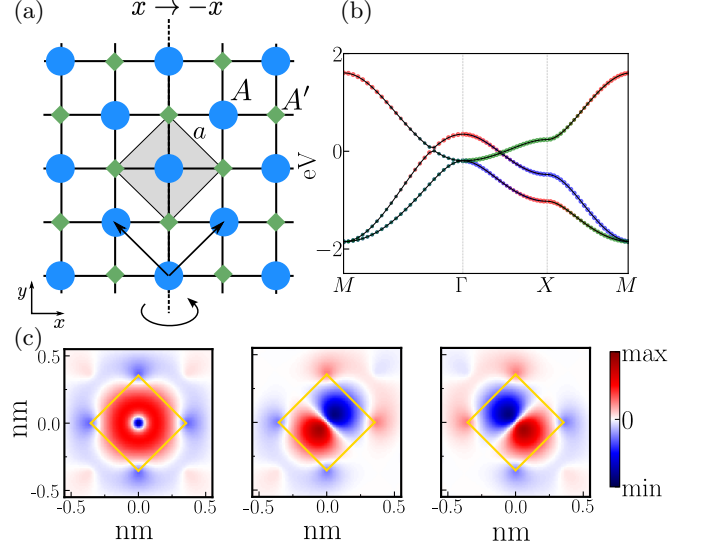


Figure 1. (a) 2D crystal structure. Big circles and small diamonds represent the positions of the two atomic-like potential wells, A and A' , respectively. The shaded area denotes the unit cell, while $a = 0.5$ nm indicates the lattice parameter. The dashed line represents the reflection symmetry broken by the excitonic instability in the channel $\Delta_+ = -i\Delta_- = \Delta$. The arrows indicate the primitive vectors of the Bravais lattice. The curved arrow indicates the wrapping around the y -axis discussed in this work. (b) Fat band representation of the low-energy band structure. The band structure is obtained by setting (see main text): $\gamma_A = 1.52$ eV nm, $\gamma_{A'} = 0.38$ eV nm, $\xi_A = \xi_{A'} = 1$ nm, and $\eta_A = \eta_{A'} = 10^{-3}$ nm. Red, green, and blue projections correspond, respectively, to the s , p_+ , and p_- Wannier orbitals. (c) Real-space maps of the s , p_+ , and p_- Wannier orbitals (from left to right).

in mind, we add to the bare band Hamiltonian \mathcal{H}_0 two electron-electron interaction contributions: i) a purely local density-density interaction U between p_+ and p_- Wannier orbitals, and ii) a density-density interaction V between s and p_{\pm} orbitals. The full Hamiltonian therefore reads:

$$\mathcal{H} = \mathcal{H}_0 + U \sum_{\mathbf{R}} n_{\mathbf{R}, p_+} n_{\mathbf{R}, p_-} + V \sum_{\mathbf{R}, \alpha = \pm} n_{\mathbf{R}, p_{\alpha}} n_{\mathbf{R}, s}. \quad (2)$$

For the sake of concreteness, we fix $U = 2.5$ eV and $V = 2.0$ eV, of the same order of magnitude of the bandwidth W .

Seeking for the excitonic instability, we introduce a family of Hartree-Fock variational wave-functions $|\Psi_{\Delta}\rangle$, which allow for a non-vanishing order parameter

$$\Delta_{\pm} \equiv \langle \Psi_{\Delta} | c_{\mathbf{R}, p_{\alpha}}^{\dagger} c_{\mathbf{R}, s} | \Psi_{\Delta} \rangle \neq 0. \quad (3)$$

By introducing Lagrange multipliers λ_{\pm} , we compute the variational energy as a function of Δ_{\pm} :

$$E_{\text{var}}[\Delta_{\pm}, \lambda_{\pm}] = \langle \Psi_{\Delta} | \mathcal{H} | \Psi_{\Delta} \rangle + \sum_{\mathbf{R}, \alpha = \pm} \lambda_{\alpha} \left(\langle \Psi_{\Delta} | c_{\mathbf{R}, p_{\alpha}}^{\dagger} c_{\mathbf{R}, s} | \Psi_{\Delta} \rangle - \Delta_{\alpha} \right) + \text{c.c.} \quad (4)$$

For a given Δ_{\pm} , we use a standard Hartree-Fock decoupling of the interaction terms and self-consistently optimize the variational wave-function with respect to the Lagrange multipliers and all the expectation values $\Delta_{\mathbf{k}}^{\alpha,\beta} = \langle \Psi_{\Delta} | c_{\mathbf{k},\alpha}^{\dagger} c_{\mathbf{k},\beta} | \Psi_{\Delta} \rangle$. We restrict our analysis to the channel $\Delta_{+} = -i\Delta_{-}$, which corresponds to the breaking of reflection symmetry $x \rightarrow -x$ (see Fig. 1). With this choice, the energy functional in Eq. (4) reduces to a function of a single order parameter $\Delta \equiv \Delta_{+}$.

In Fig. 2(a) we plot the energy landscape as a function of the real and imaginary parts of the order parameter Δ . We clearly see two equivalent global minima for the case of a purely real order parameter, which reflects the Z_2 nature of the symmetry $x \rightarrow -x$. We compute the charge $\rho_{\Delta}(\mathbf{x}) \equiv \langle \Psi_{\Delta} | \Psi^{\dagger}(\mathbf{x}) \Psi(\mathbf{x}) | \Psi_{\Delta} \rangle$ and momentum $\mathbf{p}_{\Delta}(\mathbf{x}) \equiv \frac{1}{2} \langle \Psi_{\Delta} | \Psi^{\dagger}(\mathbf{x}) \mathbf{p} \Psi(\mathbf{x}) | \Psi_{\Delta} \rangle + \text{c.c.}$ densities by expanding the fermionic fields over the complete set of Bloch wave-functions $\Psi(\mathbf{x}) = \sum_{\mathbf{k},n} \psi_{\mathbf{k},n}(\mathbf{x}) c_{\mathbf{k},n}$. In Fig. 2(b), we plot the charge density at the global minimum $\varphi = 0$ and for $|\Delta| = 0.25$. The breaking of the reflection symmetry, manifested by $\rho_{\Delta}(x, y) \neq \rho_{\Delta}(-x, y)$, is evident. The momentum density at the global minimum (not shown) is zero everywhere. We therefore conclude that the two global minima occurring for $\text{Im}(\Delta) = 0$ correspond to *pure* CDSB states. In Fig. 2(c) we show the momentum density $\mathbf{p}_{\Delta}(\mathbf{x})$ of the unstable state for $\varphi = \pi/2$ and same value of $|\Delta|$. We clearly see that the momentum density features two counter-rotating vortices, showing the TRSB nature of the excited $\varphi = \pi/2$ state.

We quantify the CDSB and TRSB character of a generic state $|\Psi_{\Delta}\rangle$ by computing the quantities $\delta\rho \equiv \int_{x<0} \rho_{\Delta}(\mathbf{x}) d^2\mathbf{x} - \int_{x>0} \rho_{\Delta}(\mathbf{x}) d^2\mathbf{x}$ and $\mathbf{P} \equiv \int_{x<0} \mathbf{p}_{\Delta}(\mathbf{x}) d^2\mathbf{x} + \int_{x>0} \mathbf{p}_{\Delta}(\mathbf{x}) d^2\mathbf{x}$, where “ $\int_{x</>0}$ ” means integration over the two portions of the unit cells separated by the $x = 0$ axis. Moving away from the global minimum at $\varphi = 0$, the CDSB contribution $\delta\rho$ decreases and vanishes for $\varphi = \pi/2$, where the TRSB contribution \mathbf{P} is maximum—see Fig. 2(d). We notice that the TRSB excitonic state corresponds to a net momentum through the unit cell along the x direction. On the contrary, the net momentum along the y direction is identically zero.

TRSB Excitonic state.—All the TRSB states obtained by the variational optimization of Eq. (4) are unstable, meaning that the purely electronic features no stable local minimum other than the two global ones for $\varphi = 0, \pi$. Physically, we expect the energy of the TRSB state to be lowered by a magnetic flux. Indeed, in nature, a current acts as source of a magnetic flux. It means that, from the point of view of the energetic gain, the energy of the TRSB state including the flux sourced by the TRSB state itself should have energy lower than the energy of the TRSB state without self-generated flux.

We investigate the magnetostatic energy lowering of the TRSB state by wrapping the 2D system on a cylinder of radius L around the y -axis—see Fig. 1(a). We also

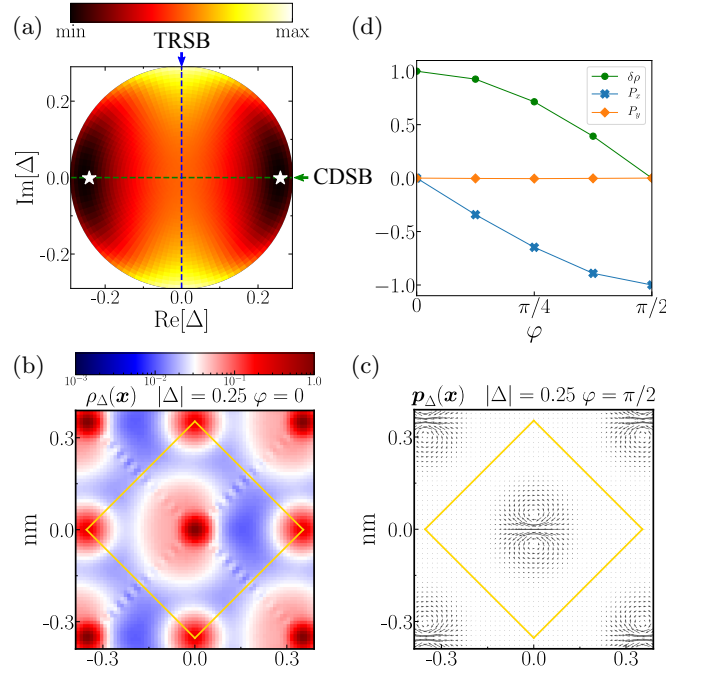


Figure 2. (a) Variational energy for the pure electronic problem as a function of $\text{Re}(\Delta)$ and $\text{Im}(\Delta)$. The white stars indicate the two global minima while the dashed horizontal (vertical) line highlights the purely CDSB (TRSB) state. (b) Quantifiers $\delta\rho$ and \mathbf{P} (see main text) of the CDSB and TRSB character of a generic state $|\Psi_{\Delta}\rangle$ at a fixed value of $|\Delta| = 0.25$ and varying phase φ . $\delta\rho$ is measured with respect to its $\varphi = 0$ value, whereas $P_{x/y}$ components are measured with respect to their $\varphi = \pi/2$ values. (c) Spatial map of the charge density $\rho_{\Delta}(\mathbf{x})$ for $\text{Re}(\Delta) = 0.25$ and $\text{Im}(\Delta) = 0$. The charge density is measured with respect to its maximum. (d) Spatial map of the momentum density \mathbf{p}_{Δ} for $\text{Re}(\Delta) = 0$ and $\text{Im}(\Delta) = 0.25$.

assume that $L \gg a$, so that the cylinder is equivalent to a 2D system with periodic boundary conditions. We introduce a new energy functional $\mathcal{E}[\Delta, \mathbf{A}, \lambda]$ which depends on the excitonic order parameter Δ , the associated Lagrange parameter λ , and on a self-generated, purely transverse ($\nabla \cdot \mathbf{A} = 0$), vector potential \mathbf{A}

$$\begin{aligned} \mathcal{E}[\Delta, \mathbf{A}, \lambda] = & E_{\text{var}}[\Delta, \lambda] + \int_{\mathbf{v}} d^3\mathbf{r} \frac{[\nabla \times \mathbf{A}(\mathbf{r})]^2}{2\mu_0} + \\ & + \frac{e}{m} \int_{\mathbf{s}} d^2\mathbf{x} \mathbf{p}_{\Delta}(\mathbf{x}) \cdot \mathbf{A}(\mathbf{x}) + \\ & + \frac{e^2}{2m} \int_{\mathbf{s}} d^2\mathbf{x} \rho_{\Delta}(\mathbf{x}) \mathbf{A}^2(\mathbf{x}), \end{aligned} \quad (5)$$

where m is the bare electron mass in vacuum, μ_0 is the vacuum magnetic permeability, and $\int_{\mathbf{v}} d^3\mathbf{r}$ ($\int_{\mathbf{s}} d^2\mathbf{x}$) indicates the volume (surface) integral over the full space (restricted to cylinder).

Imposing that \mathcal{E} is stationary with respect to the vector potential, i.e. $\delta\mathcal{E}/\delta\mathbf{A} = 0$, yields Ampere's law:

$$-\nabla^2 \mathbf{A} = \mu_0 \mathbf{J}[\mathbf{A}, \Delta], \quad (6)$$

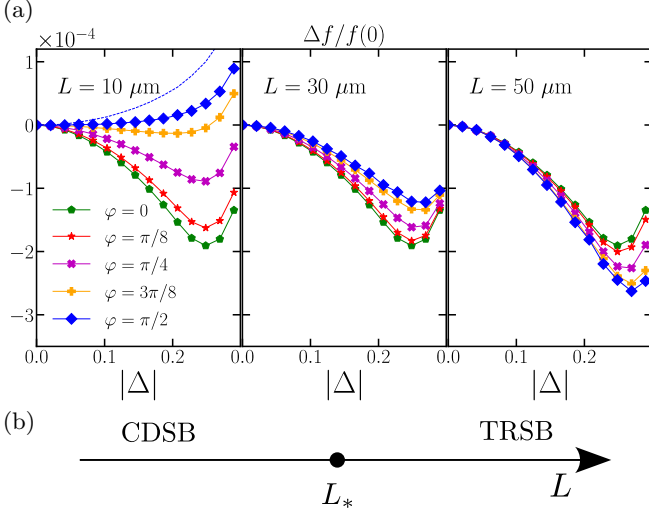


Figure 3. (a) Volume energy density $f(\Delta)$ as a function of $|\Delta|$, for different values of φ —from the pure CDSB (green pentagons) state at $\varphi = 0$ to the pure TRSB (blue diamonds) state at $\varphi = \pi/2$ —and different values of the cylinder radius L . All the energies are measured with respect to the energy $f(0)$ in the $\Delta = 0$ symmetric case— $\Delta f \equiv f(\Delta) - f(0)$ —and in units of $f(0)$. In the $L = 10 \mu\text{m}$ panel the dashed line represents the energy density for the $\pi/2$ state for the purely electronic problem in the absence of self-generated flux. (b) Schematic phase diagram as a function of the cylinder radius L : for $L > L_*$ the TRSB state becomes the ground state.

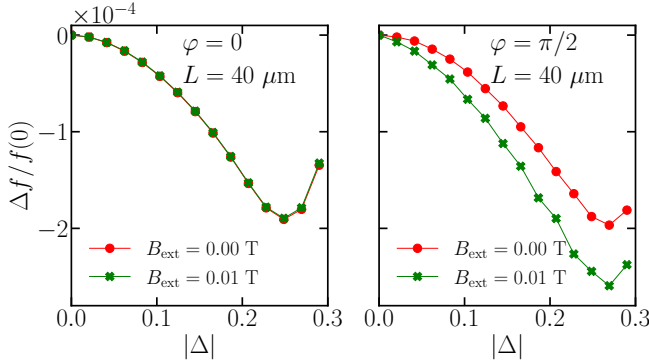


Figure 4. Volume energy density of the pure CDSB state (left) and the pure TRSB state (right) as a function of an applied external flux.

where, in cylindrical coordinates $\mathbf{r} = (r, \varphi, y)$, the volume current density reads

$$\mathbf{J}[\mathbf{A}, \Delta] = -\frac{e}{m} \delta(r - L) [\mathbf{p}_\Delta(\mathbf{x}) + e\rho_\Delta(\mathbf{x})\mathbf{A}(\mathbf{r})], \quad (7)$$

$\mathbf{x} = (L \sin \varphi, L \cos \varphi, y)$ being a point on the cylinder surface.

Solving Eq. (6) allows to eliminate \mathbf{A} and express the energy \mathcal{E} as a function of Δ only. To this extent, we coarse grain the charge and momentum density by averaging over the unit cell. In doing so, we obtain a TRSB state with a uniform charge density ρ_0 and a uniform

solenoidal momentum density $\mathbf{p}_\Delta = \varphi P_\Delta$. This approximation corresponds to neglecting contributions of the flux which are i) perpendicular to the cylinder surface and ii) vary over length scales smaller than the lattice parameter. We get a constant solenoidal vector potential $\mathbf{A}(\mathbf{r}) = \varphi A_\Delta [(L/r)\theta(r - L) + (r/L)\theta(L - r)]$, where

$$A_\Delta = -\Phi_0 \frac{P_\Delta}{h\rho_0} \frac{L}{\ell_0 + L}. \quad (8)$$

Here, $\Phi_0 = h/e$ is the flux quantum, and $\ell_0 \equiv 2m/(\mu_0 e^2 \rho_0) \simeq 3.5 \mu\text{m}$ is a characteristic length scale of the problem set by the electronic density $\rho_0 = 4/a^2$. In Eq. (8), P_Δ is the average momentum density computed for the variational state $|\Psi_\Delta\rangle$, and in the presence of the solenoidal vector potential A_Δ . We solve Eq. (8) self-consistently, together with the optimization of the Lagrange parameter and the variational wave-function $|\Psi_\Delta\rangle$ [27]. We obtain the total volume energy density $f(\Delta) \equiv \mathcal{E}/(\pi L^2 L_z)$ as a function of the order parameter, where the limit of an infinitely-long cylinder $L_z \rightarrow \infty$ is understood.

The energy lowering of a TRSB state due to the sourcing of the vector potential is expected to increase with the ratio $\ell \equiv L/\ell_0$. Indeed, by considering the electronic kinetic energy $E_{\text{kin}} \propto \langle (P + eA)^2 \rangle$, the vector potential yields a negative contribution $\Delta E_{\text{kin}} \sim -P_\Delta^2 \left(\frac{L}{\ell_0 + L} \right)^2$ which increases with the average momentum density, and, for fixed P_Δ , with the radius L . In particular, we expect a negligible contribution for cylinders of radius $L \ll \ell_0$. On the other hand, the kinetic energy gain is balanced by the positive magnetostatic energy per unit volume which, for fixed P_Δ , decreases as a function of L/ℓ_0 .

We confirm the above expectations by plotting in Fig. 3 the total energy density for increasing cylinder radius. The energy of the pure CDSB state does not depend on the cylinder radius. On the contrary, the TRSB states experience an energy lowering which increases as a function of L . As the radius of the solenoid increases, the energy minimum shifts from the CDSB state to the TRSB state for $L > L_*$, with a critical radius $L_* \approx 40 \mu\text{m}$. In the TRSB state, the solenoid is characterized a macroscopic magnetic moment sustained by a ground-state persistent current. The persistent current is a direct manifestation of the spontaneous breaking of the crystal symmetry due to the excitonic instability. In Fig. 4 we show that an external flux can further lower the energy barrier between the CDSB and TRSB states, thus highlighting the possibility of tuning the critical radius L_* .

Conclusions.—We have shown a controlled path to the stabilization of a spontaneous TRSB phase of purely orbital character issuing from an excitonic instability. The TRSB state is achieved by the engineered geometrical constraints on the system and is enabled by the direct coupling between an excitonic order parameter and the

magnetostatic degrees of freedom of the free-space electromagnetic field. The self-generated solenoidal vector potential corresponds to a macroscopic number of photons in the ground state which populate an infinite set of electromagnetic modes. In this respect, our results clarify recent discussions about superradiant and excitonic phase transitions [32] and related no-go theorems [33, 34]. Most importantly, our results suggest a novel route for the disentangling of excitonic and structural phase transitions. The TRSB is completely charge symmetric and, in contrast to the CDSB state, is expected to have no direct coupling with lattice distortions. Estimating the relative energy gain between the lattice distortion and the flux generation discussed here is beyond the scope of this work. Nonetheless, the control of the energy barrier between the TRSB and CDSB states with an external flux—see Fig. 4—highlights the intriguing possibility of a magnetostatic tuning of coupled structural and excitonic phase transition. The specific geometrical and material realizations represent interesting future research directions. This may include, for example, the interplay between geometrical constraints discussed here and the structured electromagnetic vacuum inside chiral cavities [35].

The experimental discovery of excitonic TRSB phases would provide us with an entirely new family of quantum systems displaying non-trivial time-reversal symmetry breaking of orbital origin, together with e.g. Chern insulators (such as those recently discovered in twisted bilayer graphene [36–40] and ABC-trilayer graphene [41]) and chiral superconductors (see, for example, Refs. 42–46 and references therein).

Acknowledgements.— This work was funded by the Swiss National Science Foundation through an AMBIZIONE grant (#PZ00P2.186145). G.M. acknowledges support of the MUR - Italian Minister of University and Research under the “Rita Levi-Montalcini” program. M.P. is supported by the European Union’s Horizon 2020 research and innovation programme under grant agreement No. 881603 - GrapheneCore3, by the University of Pisa under the “PRA - Progetti di Ricerca di Ateneo” (Institutional Research Grants) - Project No. PRA.2020-2021.92 “Quantum Computing, Technologies and Applications”, and by the MUR - Italian Minister of University and Research under the “Research projects of relevant national interest - PRIN 2020” - Project No. 2020JLZ52N, title “Light-matter interactions and the collective behavior of quantum 2D materials (q-LIMA)”.

It is a great pleasure to thank Antoine Georges and Aharon Kapitulnik for inspiring discussions.

* giacomo.mazza@unipi.it

[1] J. P. Eisenstein and A. H. MacDonald, *Nature* **432**, 691

- (2004).
- [2] J. P. Eisenstein, *Annu. Rev. Condens. Matter Phys.* **5**, 159 (2014).
- [3] J.-J. Su and A. H. MacDonald, *Nat. Phys.* **4**, 799 (2008).
- [4] X. Liu, K. Watanabe, T. Taniguchi, B. I. Halperin, and P. Kim, *Nat. Phys.* **13**, 746 (2017).
- [5] J. I. A. Li, T. Taniguchi, K. Watanabe, J. Hone, and C. R. Dean, *Nat. Phys.* **13**, 751 (2017).
- [6] G. W. Burg, N. Prasad, K. Kim, T. Taniguchi, K. Watanabe, A. H. MacDonald, L. F. Register, and E. Tutuc, *Phys. Rev. Lett.* **120**, 177702 (2018).
- [7] A. Kogar, M. S. Rak, S. Vig, A. A. Husain, F. Flicker, Y. Il Joe, L. Venema, G. J. MacDougall, T. C. Chiang, E. Fradkin, J. van Wezel, and P. Abbamonte, *Science* **358**, 1314 (2017).
- [8] H. Cercellier, C. Monney, F. Clerc, C. Battaglia, L. Despont, M. G. Garnier, H. Beck, P. Aebi, L. Patthey, H. Berger, and L. Forró, *Phys. Rev. Lett.* **99**, 146403 (2007).
- [9] Y. F. Lu, H. Kono, T. I. Larkin, A. W. Rost, T. Takayama, A. V. Boris, B. Keimer, and H. Takagi, *Nat. Commun.* **8**, 14408 (2017).
- [10] S. S. Ataie, D. Varsano, E. Molinari, and M. Rontani, *Proc. Natl. Acad. Sci. (USA)* **118**, e2010110118 (2021).
- [11] B. Sun, W. Zhao, T. Palomaki, Z. Fei, E. Runburg, P. Malinowski, X. Huang, J. Cenker, Y.-T. Cui, J.-H. Chu, X. Xu, S. S. Ataie, D. Varsano, M. Palummo, E. Molinari, M. Rontani, and D. H. Cobden, *Nat. Phys.* **18**, 94 (2022).
- [12] D. Varsano, M. Palummo, E. Molinari, and M. Rontani, *Nat. Nanotech.* **15**, 367 (2020).
- [13] G. Mazza, M. Rösner, L. Windgätter, S. Latini, H. Hübener, A. J. Millis, A. Rubio, and A. Georges, *Phys. Rev. Lett.* **124**, 197601 (2020).
- [14] T. Kaneko, T. Toriyama, T. Konishi, and Y. Ohta, *Phys. Rev. B* **87**, 035121 (2013).
- [15] M. D. Watson, I. Marković, E. A. Morales, P. Le Fèvre, M. Merz, A. A. Haghighirad, and P. D. C. King, *Phys. Rev. Research* **2**, 013236 (2020).
- [16] L. Windgätter, M. Rösner, G. Mazza, H. Hübener, A. Georges, A. J. Millis, S. Latini, and A. Rubio, *npj Comput. Mater.* **7**, 210 (2021).
- [17] A. Subedi, *Phys. Rev. Materials* **6**, 014602 (2022).
- [18] K. Kim, H. Kim, J. Kim, C. Kwon, J. S. Kim, and B. J. Kim, *Nat. Commun.* **12**, 2998 (2021).
- [19] M. Ye, P. A. Volkov, H. Lohani, I. Feldman, M. Kim, A. Kanigel, and G. Blumberg, *Phys. Rev. B* **104**, 045102 (2021).
- [20] D. Golež, S. K. Y. Dufresne, M.-J. Kim, F. Boschini, H. Chu, Y. Murakami, G. Levy, A. K. Mills, S. Zhdanovich, M. Isobe, H. Takagi, S. Kaiser, P. Werner, D. J. Jones, A. Georges, A. Damascelli, and A. J. Millis, *Phys. Rev. B* **106**, L121106 (2022).
- [21] K. Katsumi, A. Alekhin, S.-M. Souliou, M. Merz, A.-A. Haghighirad, M. Le Tacon, S. Houver, M. Cazayous, A. Sacuto, and Y. Gallais, *arXiv:2211.08537*.
- [22] M. Michael, S. R. Ul Haque, L. Windgätter, S. Latini, Y. Zhang, A. Rubio, R. D. Averitt, and E. Demler, *arXiv:2207.08851*.
- [23] B. A. Volkov and Yu. V. Kopayev, *JETP* **27**, 7 (1978).
- [24] B. A. Volkov, V. L. Ginzburg, and Yu. V. Kopayev, *JETP* **27**, 206 (1978).
- [25] A. Amaricci, G. Mazza, M. Capone, and M. Fabrizio, *arXiv:2212.05878*.
- [26] N. Marzari, A. A. Mostofi, J. R. Yates, I. Souza, and D.

- Vanderbilt, *Rev. Mod. Phys.* **84**, 1419 (2012).
- [27] See the Supplemental Material file, which contains details on the variational wave-function optimization and citations to Ref. [28–31]
- [28] Jiajun Li, Denis Golez, Giacomo Mazza, Andrew J. Millis, Antoine Georges, and Martin Eckstein. *Phys. Rev. B* **101**, 205140 (2020).
- [29] Omar Di Stefano, Alessio Settineri, Vincenzo Macrì, Luigi Garziano, Roberto Stassi, Salvatore Savasta, and Franco Nori. *Nat. Phys.* **15**, 8 (2019).
- [30] Ivan Amelio, Lukas Korosec, Iacopo Carusotto, and Giacomo Mazza. *Phys. Rev. B* **104**, 235120 (2021).
- [31] Olesia Dmytruk and Marco Schiró. *Phys. Rev. B* **103**, 075131 (2021).
- [32] G. Mazza and A. Georges, *Phys. Rev. Lett.* **122**, 017401 (2019).
- [33] G. M. Andolina, F. M. D. Pellegrino, V. Giovannetti, A. H. MacDonald, and M. Polini, *Phys. Rev. B* **100**, 121109 (2019).
- [34] G. M. Andolina, F. M. D. Pellegrino, A. Mercurio, O. Di Stefano, M. Polini, and S. Savasta, *Eur. Phys. J. Plus* **137**, 1348 (2022).
- [35] H. Hübener, U. De Giovannini, C. Schäfer, J. Andberger, M. Ruggenthaler, J. Faist, and A. Rubio, *Nat. Mater.* **20**, 438 (2021).
- [36] M. Serlin, C. L. Tschirhart, H. Polshyn, Y. Zhang, J. Zhu, K. Watanabe, T. Taniguchi, L. Balents, and A. F. Young, *Science* **367**, 900 (2019).
- [37] C. L. Tschirhart, M. Serlin, H. Polshyn, A. Shragai, Z. Xia, J. Zhu, Y. Zhang, K. Watanabe, T. Taniguchi, M. E. Huber, and A. F. Young, *Science* **372**, 1323 (2021).
- [38] K. P. Nuckolls, M. Oh, D. Wong, B. Lian, K. Watanabe, T. Taniguchi, B. A. Bernevig, and A. Yazdani, *Nature* **588**, 610 (2020).
- [39] P. Stepanov, M. Xie, T. Taniguchi, K. Watanabe, X. Lu, A. H. MacDonald, B. A. Bernevig, and D. K. Efetov, *Phys. Rev. Lett.* **127**, 197701 (2021).
- [40] Y. Xie, A. T. Pierce, J. M. Park, D. E. Parker, E. Khalaf, P. Ledwith, Y. Cao, S. H. Lee, S. Chen, P. R. Forrester, K. Watanabe, T. Taniguchi, A. Vishwanath, P. Jarillo-Herrero, and A. Yacoby, *Nature* **600**, 439 (2021).
- [41] G. Chen, A. L. Sharpe, E. J. Fox, Y.-H. Zhang, S. Wang, L. Jiang, B. Lyu, H. Li, K. Watanabe, T. Taniguchi, Z. Shi, T. Senthil, D. Goldhaber-Gordon, Y. Zhang, and F. Wang, *Nature* **579**, 56 (2020).
- [42] J. Xia, Y. Maeno, P. T. Beyersdorf, M. M. Fejer, and A. Kapitulnik, *Phys. Rev. Lett.* **97**, 167002 (2006).
- [43] G. E. Volovik, *The Universe in a Helium Droplet* (Oxford University Press, Oxford, 2003).
- [44] B. A. Bernevig and T. L. Hughes, *Topological Insulators and Superconductors* (Princeton University Press, Princeton, 2013)
- [45] X.-L. Qi and S.-C. Zhang, *Rev. Mod. Phys.* **83**, 1057 (2011).
- [46] C. Kallin and J. Berlinsky, *Rep. Prog. Phys.* **79**, 054502 (2016).

Supplemental material: A geometric path towards excitonic insulators with purely orbital time-reversal symmetry breaking

Giacomo Mazza^{1,2,*} and Marco Polini^{1,3,4}

¹*Dipartimento di Fisica dell'Università di Pisa, Largo Bruno Pontecorvo 3, I-56127 Pisa, Italy*

²*Department of Quantum Matter Physics, University of Geneva,
Quai Ernest-Ansermet 24, 1211 Geneva, Switzerland*

³*Istituto Italiano di Tecnologia, Graphene Labs, Via Morego 30, I-16163 Genova, Italy*

⁴*ICFO-Institut de Ciències Fotòniques, The Barcelona Institute of Science and Technology,
Av. Carl Friedrich Gauss 3, 08860 Castelldefels (Barcelona), Spain*

MODEL OF INTERACTING ELECTRONS ON A SQUARE LATTICE

We consider a periodic potential on a square lattice defined by the primitive vectors

$$\mathbf{a}_1 = \frac{a}{\sqrt{2}} (1, 1) , \quad \mathbf{a}_2 = \frac{a}{\sqrt{2}} (-1, 1) . \quad (1)$$

We define the crystalline potential as

$$V(\mathbf{x}) = \sum_{\mathbf{R}} \sum_{a=A,A'} v_a(\mathbf{x} - \mathbf{R}) , \quad (2)$$

where

$$v_a(\mathbf{x}) = -\gamma_a \frac{e^{-|\mathbf{x}-\mathbf{x}_a|/\xi_a}}{|\mathbf{x}-\mathbf{x}_a| + \eta_a} , \quad \mathbf{x}_A = (0, 0) , \quad \mathbf{x}_{A'} = \frac{\mathbf{a}_1 + \mathbf{a}_2}{2} . \quad (3)$$

We solve the Schrodinger equation for electrons in such a periodic potential by using a plane wave expansion and obtain Bloch wave-functions $|\mathbf{k}n\rangle$:

$$\frac{\hbar^2}{2m} (\mathbf{k} + \mathbf{G})^2 u_{\mathbf{k}n}(\mathbf{G}) + \sum_{\mathbf{G}'} V_{\mathbf{G}\mathbf{G}'} u_{\mathbf{k}n}(\mathbf{G}') = E_{\mathbf{k}n} u_{\mathbf{k}n}(\mathbf{G}) , \quad (4)$$

where m is the bare electron's mass in vacuum, $u_{\mathbf{k}n}(\mathbf{G})$ is the Fourier transform of the periodic part $u_{\mathbf{k}n}(\mathbf{x})$ of the Bloch wave-function, and $V_{\mathbf{G}\mathbf{G}'} = \int d^2\mathbf{x} e^{i(\mathbf{G}-\mathbf{G}')\cdot\mathbf{x}} V(\mathbf{x})$. In the plane-wave expansion we use an energy cut-off $E_{\text{PW}} = 900$ eV.

By assuming $N = 4$ spinless electrons per unit cell, the three bands close to the Fermi level have character of the 2 s and 1 p_{\pm} orbitals of the central atom. We extract Wannier wave-functions $|\Psi_{\mathbf{k}\alpha}\rangle$, $\alpha = s, p_{\pm}$, by projecting over atomic orbitals:

$$|\Psi_{\mathbf{k}\alpha}\rangle = \sum_n |\mathbf{k}n\rangle [U(\mathbf{k})]_{n\alpha} , \quad [U(\mathbf{k})]_{n\alpha} = \left[A_{\mathbf{k}} \left(A_{\mathbf{k}}^{\dagger} A_{\mathbf{k}} \right)^{-1/2} \right]_{n\alpha} , \quad (5)$$

where $(A_{\mathbf{k}})_{n\alpha} = \langle \mathbf{k}n | \phi_{\alpha} \rangle$ is the projection of the Bloch state $|\mathbf{k}n\rangle$ onto the atomic orbital $|\phi_{\alpha}\rangle$, $\alpha = s, p_{\pm}$, and $U(\mathbf{k})$ is a unitary transformation. We therefore arrive at the non interacting Hamiltonian in the Wannier basis:

$$\mathcal{H}_0 = \sum_{\mathbf{R}\mathbf{R}'} \sum_{\alpha\beta} h_{\mathbf{R}\mathbf{R}'}^{\alpha\beta} c_{\mathbf{R}\alpha}^{\dagger} c_{\mathbf{R}'\beta} . \quad (6)$$

ENERGY OPTIMIZATION FOR THE PURELY ELECTRONIC MODEL

The variational energy for the purely electronic model reads

$$E_{\text{var}}[\Delta_{\pm}, \lambda_{\pm}] = \langle \Psi_{\Delta} | \mathcal{H} | \Psi_{\Delta} \rangle + \sum_{\mathbf{R}} \sum_{\alpha=\pm} \lambda_{\alpha} \left(\langle \Psi_{\Delta} | c_{\mathbf{R},p_{\alpha}}^{\dagger} c_{\mathbf{R},s} | \Psi_{\Delta} \rangle - \Delta_{\alpha} \right) + \text{c.c.} . \quad (7)$$

We use Wick's theorem to decouple the expectation values of many-body terms computed on the Hartree-fock wave-function:

$$\langle \Psi_\Delta | c_\alpha^\dagger c_\alpha c_\beta^\dagger c_\beta | \Psi_\Delta \rangle = \langle \Psi_\Delta | c_\alpha^\dagger c_\alpha | \Psi_\Delta \rangle \langle \Psi_\Delta | c_\beta^\dagger c_\beta | \Psi_\Delta \rangle - \langle \Psi_\Delta | c_\alpha^\dagger c_\beta | \Psi_\Delta \rangle \langle \Psi_\Delta | c_\beta^\dagger c_\alpha | \Psi_\Delta \rangle , \quad (8)$$

and obtain

$$\begin{aligned} E_{\text{var}}[\Delta_\pm, \lambda_\pm] = & \sum_{\mathbf{k}} \sum_{\alpha\beta} h_{\mathbf{k}}^{\alpha\beta} \langle \Psi_\Delta | c_{\mathbf{k}\alpha}^\dagger c_{\mathbf{k}\beta} | \Psi_\Delta \rangle + \sum_{\mathbf{R}\alpha=\pm} \lambda_\alpha \left(\langle \Psi_\Delta | c_{\mathbf{R}p_\alpha}^\dagger c_{\mathbf{R}s} | \Psi_\Delta \rangle - \Delta_\alpha \right) + \text{c.c.} + \\ & + U \sum_{\mathbf{R}} \langle \Psi_\Delta | c_{\mathbf{R}p_+}^\dagger c_{\mathbf{R}p_+} | \Psi_\Delta \rangle \langle \Psi_\Delta | c_{\mathbf{R}p_-}^\dagger c_{\mathbf{R}p_-} | \Psi_\Delta \rangle - U \sum_{\mathbf{R}} \langle \Psi_\Delta | c_{\mathbf{R}p_+}^\dagger c_{\mathbf{R}p_-} | \Psi_\Delta \rangle \langle \Psi_\Delta | c_{\mathbf{R}p_-}^\dagger c_{\mathbf{R}p_+} | \Psi_\Delta \rangle + \\ & + V \sum_{\mathbf{R}\alpha=\pm} \langle \Psi_\Delta | c_{\mathbf{R}s}^\dagger c_{\mathbf{R}s} | \Psi_\Delta \rangle \langle \Psi_\Delta | c_{\mathbf{R}p_\alpha}^\dagger c_{\mathbf{R}p_\alpha} | \Psi_\Delta \rangle - V \sum_{\mathbf{R}\alpha=\pm} \langle \Psi_\Delta | c_{\mathbf{R}s}^\dagger c_{\mathbf{R}p_\alpha} | \Psi_\Delta \rangle \langle \Psi_\Delta | c_{\mathbf{R}p_\alpha}^\dagger c_{\mathbf{R}s} | \Psi_\Delta \rangle . \quad (9) \end{aligned}$$

Energy minimization implies that $|\Psi_\Delta\rangle$ is the ground state of the self-consistent Hartree-Fock Hamiltonian \mathcal{H}_{HF} :

$$\hat{\mathcal{H}}_{\text{HF}} |\Psi_\Delta\rangle = E_{\text{HF}} |\Psi_\Delta\rangle , \quad (10)$$

where

$$\begin{aligned} \hat{\mathcal{H}}_{\text{HF}} = & \sum_{\mathbf{k}} \sum_{\alpha\beta} h_{\mathbf{k}}^{\alpha\beta} c_{\mathbf{k}\alpha}^\dagger c_{\mathbf{k}\beta} + \sum_{\mathbf{R}\alpha} \lambda_\alpha c_{\mathbf{R}p_\alpha}^\dagger c_{\mathbf{R}s} + \text{H.c.} + \\ & + U \sum_{\mathbf{R}} \left[\langle n_{\mathbf{R}p_+} \rangle c_{\mathbf{R}p_-}^\dagger c_{\mathbf{R}p_-} + \langle n_{\mathbf{R}p_-} \rangle c_{\mathbf{R}p_+}^\dagger c_{\mathbf{R}p_+} \right] - U \sum_{\mathbf{R}} \left[\langle c_{\mathbf{R}p_+}^\dagger c_{\mathbf{R}p_-} \rangle c_{\mathbf{R}p_+} c_{\mathbf{R}p_-}^\dagger + \text{H.c.} \right] \\ & + V \sum_{\mathbf{R}\alpha=\pm} \left[\langle n_{\mathbf{R}p_\alpha} \rangle c_{\mathbf{R}s}^\dagger c_{\mathbf{R}s} + \langle n_{\mathbf{R}s} \rangle c_{\mathbf{R}p_\alpha}^\dagger c_{\mathbf{R}p_\alpha} \right] - V \sum_{\mathbf{R}\alpha=\pm} \left[\langle c_{\mathbf{R}p_\alpha}^\dagger c_{\mathbf{R}s} \rangle c_{\mathbf{R}s} c_{\mathbf{R}p_\alpha}^\dagger + \text{H.c.} \right] . \quad (11) \end{aligned}$$

We solve the eigenvalue problem in Eq. (10) in a self-consistent manner. At each iteration of the self-consistent loop, λ_\pm is fixed by solving the equation

$$\langle \Psi_\Delta | c_{\mathbf{R}p_\alpha}^\dagger c_{\mathbf{R}s} | \Psi_\Delta \rangle = \Delta_\alpha . \quad (12)$$

Once the variational wave-function is optimized, the variational energy reads:

$$E_{\text{var}} = E_{\text{HF}} - U \sum_{\mathbf{R}} \langle n_{p_+} \rangle \langle n_{p_-} \rangle - V \sum_{\mathbf{R}\alpha} \langle n_{p_\alpha} \rangle \langle n_s \rangle + U \sum_{\mathbf{R}} |\langle c_{p_+}^\dagger c_{p_-} \rangle|^2 + V \sum_{\mathbf{R}\alpha} |\langle c_{p_\alpha}^\dagger c_s \rangle|^2 . \quad (13)$$

ENERGY OPTIMIZATION WITH SELF-GENERATED VECTOR POTENTIAL IN SOLENOIDAL GEOMETRY

The solution of the Ampere's equation with coarse grained momentum and charge densities gives rise to the purely solenoidal vector potential $\mathbf{A} = \boldsymbol{\varphi} A_\Delta$, where the expression of A_Δ is reported in the main text.

We consider a cylinder of radius $L \gg a$. In this limit, the electronic problem on the cylinder can be approximated by the electronic problem on the original 2D lattice with periodic boundary conditions. In the coordinate systems of the 2D square lattice, the purely solenoidal vector potential becomes a constant vector potential directed along x , $\mathbf{A} = A(1, 0)$. The total energy is given by:

$$\mathcal{E} = E_{\text{var}} + \frac{e}{m} \sum_{\mathbf{k}} \sum_{\alpha\beta} \mathbf{p}_{\alpha\beta}(\mathbf{k}) \cdot \mathbf{A} \langle \Psi_\Delta | c_{\mathbf{k}\alpha}^\dagger c_{\mathbf{k}\beta} | \Psi_\Delta \rangle + \frac{e^2}{2m} A^2 \sum_{\mathbf{k}\alpha} \langle \Psi_\Delta | c_{\mathbf{k}\alpha}^\dagger c_{\mathbf{k}\alpha} | \Psi_\Delta \rangle + \mathcal{E}_{\text{m}} , \quad (14)$$

where E_{var} has the same form as in Eq. (13) and $\mathbf{p}_{\alpha\beta}(\mathbf{k}) = -i\hbar \langle \mathbf{k}\alpha | \nabla | \mathbf{k}\beta \rangle$ is the matrix element of the momentum operator, which we compute using the Bloch wave-functions and the Wannier rotation matrices $U(\mathbf{k})$.

We note that, once we allow for a self-generated flux, the momentum matrix elements $\mathbf{p}_{\alpha\beta}(\mathbf{k})$ couple electronic states from *all* the electronic bands, and not only electronic states belonging to the low-energy bands. In fact, it is well known that, in general, the Hamiltonian representation of the interaction between electrons and the electromagnetic field requires to expand the fermionic fields on a large subspace of electronic states [1–4].

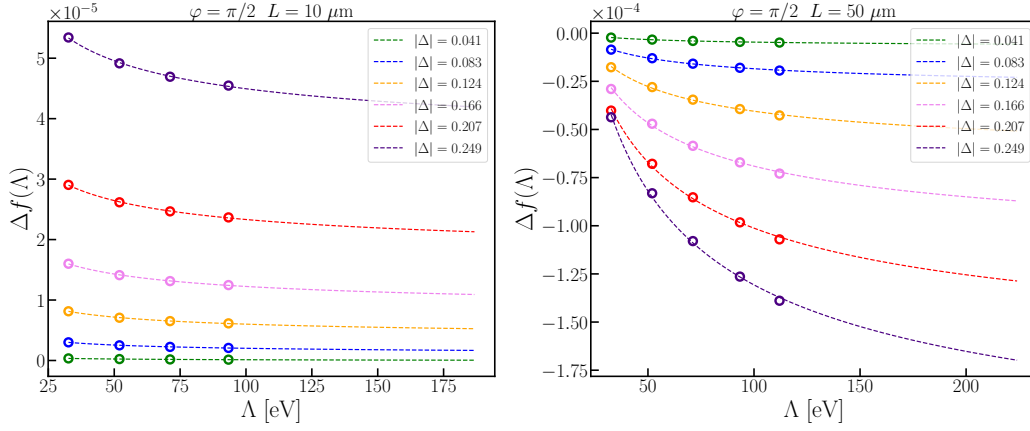


Figure 1. Examples of energy fits as functions of the cut-off Λ in the electronic bands, for the pure TRSB state (i.e. $\varphi = \pi/2$) and cylinders of radius $L = 10 \mu\text{m}$ (left) and $L = 50 \mu\text{m}$ (right). In each panel, different sets of data refer to different values $|\Delta|$ of the order parameter modulus. Dashed lines are fits with a $\Lambda^{-1/2}$ power-law decay.

Here, we tackle this problem by enlarging the electronic Hilbert space beyond the three low-energy bands considered in the purely electronic model. In practice, we keep electronic states below a cut-off energy Λ above the Fermi level, and look for convergence with respect to the cut-off. As shown in Fig. 1, the energy shows a slow convergence with respect to the energy cut-off Λ . We extrapolate the converged value by fitting the energy with the following power-law decay:

$$E(\Lambda) = E + \left[\frac{\Lambda_0}{\Lambda} \right]^\gamma. \quad (15)$$

We find that $\gamma = 0.5$ yields a good fit for all the parameters used in this work—see Fig. 1. We therefore use this parameter to extrapolate the energy. We mention that, while the precise value L_* of the CDSB to TRSB transition can depend smoothly on the procedures for energy extrapolation, the fitting procedure is not expected to affect in any significant way the qualitative picture of our results.

MAGNETIC AND ELECTRONIC ENERGY CONTRIBUTIONS TO THE TOTAL ENERGY

In this Section, we present extended data which detail the electronic and magnetic contributions to the total energy, Fig. 2. We split the variational energy into electronic and magnetic contributions:

$$\mathcal{E} = \mathcal{E}_e + \mathcal{E}_m, \quad (16)$$

where $\mathcal{E}_m = \int d^3\mathbf{r} \frac{(\nabla \times \mathbf{A})^2}{2\mu_0}$. In relation to the fitting procedure outlined above, we extrapolate independently the total volume energy density $f = \mathcal{E}/(\pi L^2 L_z)$, and the electronic surface energy density $E_e = \mathcal{E}_e/(2\pi L L_z)$. We therefore extract the magnetic volume energy density by using

$$E_m = f - \frac{2E_e}{L}. \quad (17)$$

The contributions follow the expected behaviors discussed in the main text, based on the solution of Ampere's equation, see Eq. (8) in the main text. The gain in the electronic energy becomes larger for increasing values of P_Δ (i.e. phase closer to the pure TRSB state at $\varphi = \pi/2$) and, for a fixed P_Δ (i.e. fixed phase φ), for increasing values of the cylinder radius L (see first row in Fig. 2).

The magnetic positive energy contribution is larger the closer to the pure TRSB. On the contrary, the magnetic contribution decreases with the cylinder radius (second row). This is understood as, for large L , the vector potential asymptotically cancels the momentum density P_Δ , leading to a vanishing surface current density, and, consequently, a vanishing flux density.

Eventually, the transition from the CDSB to the TRSB state is set by the balance between the energy gain in the electronic energy and the energy loss in the magnetic contribution (third row).

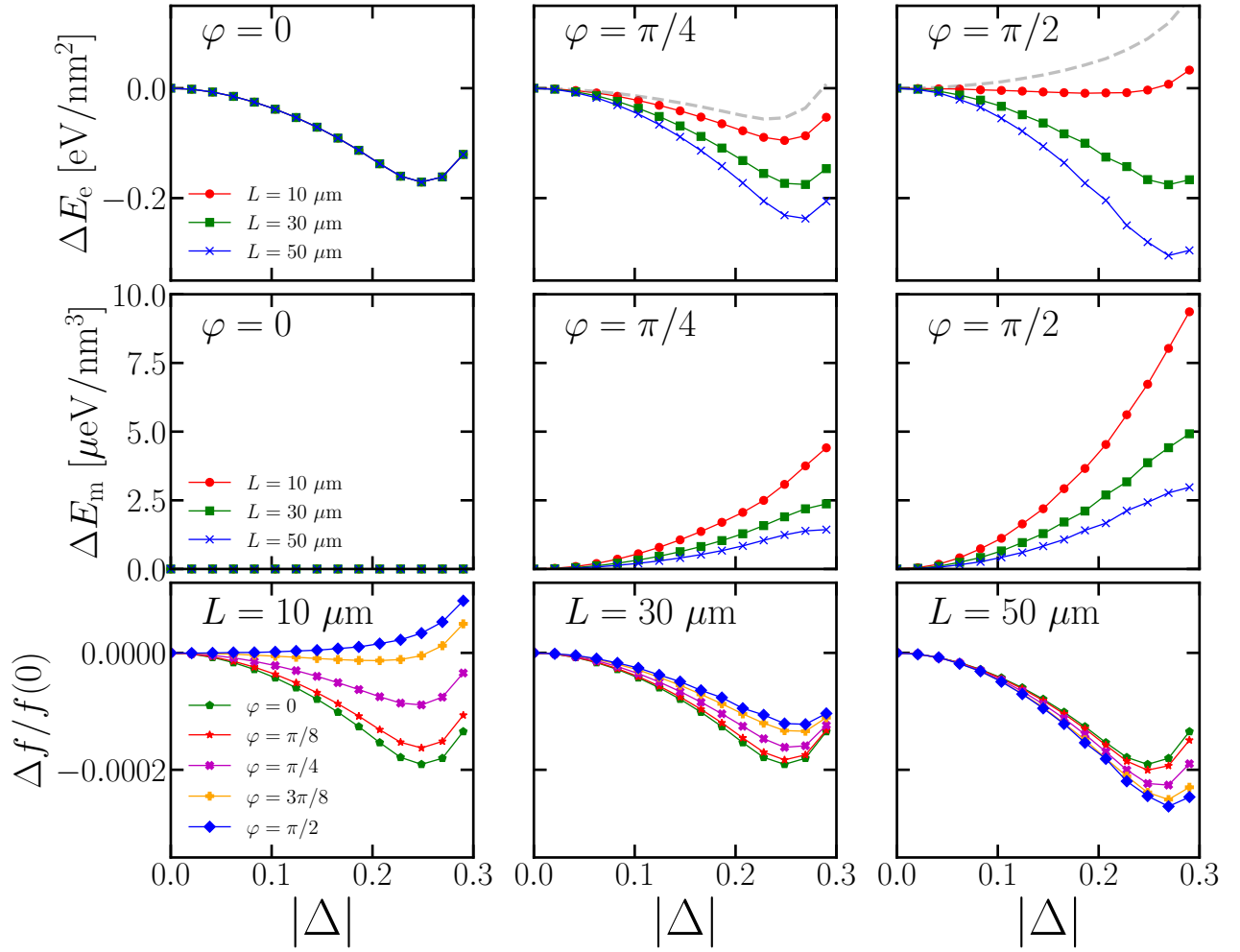


Figure 2. (First row) Electronic surface energy density for three different phases and increasing cylinder radius. For the $\varphi = \pi/4$ and $\varphi = \pi/2$ panels we report the energy of the purely electronic optimization (*i.e.* without self-generated flux) as dashed lines. (Second row) Magnetic volume energy density for the same parameters as in the first row. (Third row) Total volume energy density for different values of the cylinder radius L . (same as Fig. 3 in the main text).

* giacomo.mazza@unipi.it

- [1] Jiajun Li, Denis Golez, Giacomo Mazza, Andrew J. Millis, Antoine Georges, and Martin Eckstein. *Phys. Rev. B* **101**, 205140 (2020).
- [2] Omar Di Stefano, Alessio Settineri, Vincenzo Macrì, Luigi Garziano, Roberto Stassi, Salvatore Savasta, and Franco Nori. *Nat. Phys.* **15**, 8 (2019).
- [3] Ivan Amelio, Lukas Korosec, Iacopo Carusotto, and Giacomo Mazza. *Phys. Rev. B* **104**, 235120 (2021).
- [4] Olesia Dmytruk and Marco Schiró. *Phys. Rev. B* **103**, 075131 (2021).